ALMA Memo. No. 400
A proposal of optimized configurations for the ALMA

F. Boone

DEMIRM, Observatoire de Paris, 61 av. de l'Observatoire, 75014 Paris, France
e-mail: frederic.boone@obspm.fr

January 14, 2001

Abstract. A set of optimized configurations is presented. It results from the application of two previous papers dedicated to the design of interferometer arrays in general: the optimization of the locations of the antenna pads is performed using the Antenna Position Optimization software introduced in Boone (2001) and conforming to the analysis developed in Boone (2002). The constraints and the specifications are taken from the recommendations made at the Preliminary Design Review of February 2001 (Guilloteau & the Configuration PDR Review Committee 2001). The feasibility of a design based on an inverse approach is demonstrated. The locations of the pads are determined by the scientific goals translated in terms of target distributions of samples. The method used allows, at the same time, to control the quality of the distribution of samples (shape and minimum density of samples) and to take into account the constraints and specifications (topography, number of pads, range of resolutions). The computing time required to get a complete array is of about 3 hours on a 1 GHz PC. Rather than a fixed geometrical concept the design can therefore be seen as a numerical solution that can be re-computed for any change in the specifications or constraints.

1. Introduction

This memo describes the application of two previous papers dealing with the design of interferometer arrays in general (Boone 2001, 2002, hereafter Paper I and II), to the design of ALMA configurations. In the first paper a new method was introduced for the optimization of the antenna locations and the implementation of a software named APO was described. In the second paper an analysis was developed to determine the distributions of samples that should be taken as targets in the optimization of an array. The results of the latter reference required in this memo are gathered in Appendix A.

The optimization of the locations of the antenna pads is carried out in the frame of the recommendations made at the Preliminary Design Review of February 2001 (Guilloteau & the Configuration PDR Review Committee 2001). From this document the array should be made of: (1) a compact configuration in which the antennas are reachable with roads of 20 m in width, (2) intermediate configurations up to 3 km in baseline length, (3) an extended configuration of more than 10 km in diameter (The PDR specifies 14 km, a 10km-configuration is discussed here as a possible alternative). The total number of pads should be of about 250 and the configurations should be optimized for 60 antennas.

The aim of this memo is not only to give the resulting locations of the pads but also to describe how they were obtained. Thus, particular attention is given to the identification of the parameters that have an impact on the design and that should be determined before running the optimization.

The compact configuration rises the particular problems of shadowing and access to the antennas, it is treated in Sect.2. The sharing of the pads between the configurations is of main concern as a maximum of flexibility in resolution and sensitivity should be allowed for a total number of pads equal to 250. This problem is addressed in Sect.3. The optimization of the intermediate configurations (i.e. up to 3 km baselines) with the ground constraints of Chajnantor site is carried out in Sect.4. The optimization of the extended configuration is studied in Sect.5. Conclusions are drawn in Sect.6. In order to allow a rapid reading most of the calculations are relegated to the appendixes. All the figures are relegated to Appendix E.

2. The compact configuration

In order to minimize the shadowing the compact configuration will be mostly used for short observations around the transit. It should therefore be optimized for the mean elevation ϵ_m. The value of ϵ_m is computed in Appendix D for a uniform distribution of sources and is found equal to 60 deg. The optimization software allows to set another source elevation ϵ_{sh} that is used to constrain the shadowing: no shadowing is allowed for a source at this elevation. Following the argumentation of Appendix D it was decided to take ϵ_{sh} equal to 50 deg. Note that the software allows another mode of constraint for the shadowing: it

is possible to take several source elevations with a weight for each one and apply pressure forces on the antennas proportional to the shadowed areas.

In addition, to allow imaging with a maximum of sensitivity, the compact configuration should be optimized for a Gaussian distribution of visibilities. The lower the truncation level is, the more centrally condensed is the configuration and the higher the truncation level is, the more it resembles a ring (see Paper II). As in both cases the design prevents the access to all the antennas with a transporter, a compromise has to be found. It was found that for a truncation level of 12 dB for a maximum baseline of 200 m all the antennas were reachable with roads of 20 m in width. The duration of observation required to achieve Nyquist sampling ($\alpha = 1$ in the terminology of Paper II) with such a configuration is given by Eq.A.6 and is equal to 1.2 hours. It was chosen to optimize the configuration for this duration of observation.

The configuration was first optimized without roads, then roads of 20 m in width were added by hand within this configuration and the optimization was run again including the roads as ground constraints. The configuration and the corresponding distribution of samples are shown Fig.E.5. The dirty beam is shown in Fig.E.11 for three different kinds of weighting of the data: first natural weighting then two weightings compensating for the density excess with respect to a perfect Gaussian distribution truncated at respectively 12 dB and 20 dB (see Appendix B). The loss of sensitivity implied for the two latter cases is of respectively 5% and 10% (see Appendix C for computation). It can be noted that such a weighting allows to suppress almost completely the sidelobes due to small scale irregularities in the distribution of samples. The remaining negative bowl is due to the missing short spacings.

3. Pad sharing

In order to investigate the influence of the sampling accuracy and the truncation level demanded to the distribution of samples on the number of pads required, several arrays made of 5 configurations were optimized for various values of the sampling constraint, α, and of the truncation level specification for the Fourier transform of the clean beam, Γ_c (see the analysis developed in Paper II and summarized in Appendix A). It is reminded that that α is the maximum "distance" between the samples in Nyquist interval units that allows reliable interpolation (it is actually a question of density rather than distance and a more rigorous definition is given in Paper II). Γ_c is the level of truncation that is wanted for the Fourier transform of the clean beam (i.e. after deconvolution) called the clean weighting function.

The size of the configurations goes from 200 m (the compact configuration introduced Sect.2) to 3 km by regular increments: the length of the largest baselines of the 4 intermediate configurations are 900 m, 1600 m, 2300 m, and 3000 m. The corresponding resolutions for Γ_c =10 dB, 15 dB and 20 dB are given in Table 2. The regular increment in size is justified by the requirement that the loss of sensitivity, when degrading the resolution to an intermediate one (i.e. to a resolution that would require a configuration size between two of the four optimized ones), be minimized.

Each array optimization was carried out from the compact configuration to the most extended trying at each step to re-use the pads of the previously optimized configurations. This functionality is integrated in the software: along the optimization process, when an antenna is found near enough to an existing pad (this distance is a free parameter to be specified) it is fixed on it.

The widths of the target distributions of samples (FWHM) and the durations of the observations (Δt) are determined as described in Appendix A (Equations A.5, A.6 and A.7) and taking the parameter β equal to 1 (no extrapolation allowed) and the maximum duration of observation equal to 8 hours (justified by Fig.E.1). The values of these two parameters (FWHM and Δt) for the various configurations are shown in Table 1. It can be noted that for $\Gamma_c = 20$ dB, even for a loose constraint on the sampling ($\alpha = 4$), long track observations are always required. The declination of the source is taken as the average declination computed in Appendix D, i.e. $\delta_m = -10$ deg.

The resulting number of pads, though not representing an absolute minimum, gives an idea of the number of pads actually required to achieve the specifications. Table 3 gives the results for 9 combinations of α and Γ_c. The corresponding arrays are represented Fig.E.2 ($\alpha = 1$), Fig.E.3 ($\alpha = 2$) and Fig.E.4 ($\alpha = 4$).

It appears clearly that for a strong constraint on the sampling accuracy ($\alpha = 1$) the configurations are ring-like whatever the truncation level Γ_c specified for the clean weighting function (Fig.E.2). This comes from the fact that below 8 hours of observation there are not enough samples to achieve a Gaussian distribution truncated at the level specified by Γ_c. The sampling constraint imposes to take a flatter target distribution than the Fourier transform of the wanted beam and the flatter the distribution is the more the configuration resembles a ring. The looser the sampling constraint is (e.g. $\alpha = 4$) and the lower the truncation specification is the more centrally condensed the configurations are (the less the number of pads required) and the more the design approaches the spiral concept of Conway (2000) (see last row of Fig.E.4).

As the extended configuration should be ring-like (due to the sampling requirement), at least 50 more pads will be required and the total number of pads for the intermediate and the compact configurations should be as close as possible to 200. Then, from Table 1, the parameter α should be taken greater or equal to 4. It should be emphasized however that taking a value for α greater than 2 implies that prior information on the sources are available (e.g. the sizes of the sources are known to be less than half the size of the field of view). Without prior information mosaicing technique implies $\alpha = 2$, not more. Furthermore, in this section it was chosen to take the same sampling

Table 1. FWHM of the target distribution and duration of the observation required to achieve the specifications (α and Γ_c) for each of the four intermediate configurations. α is the constraint on the maximum distance between the samples in Nyquist interval units. Γ_c is the specification of the level of truncation of the Fourier transform of the clean beam. In each box the two parameters are given from top to bottom in crescent order of the configuration size. It is recalled that the length of the largest baseline in each of the configurations is respectively 900 m, 1600 m, 2300 m and 3000 m.

	$\alpha = 1$		$\alpha = 2$		$\alpha = 4$	
	FWHM	Δt	FWHM	Δt	FWHM	Δt
$\Gamma_c = 10$ dB	988 m	4.0 h	988 m	2.0 h	988 m	1.0 h
	1756 m	7.1 h	1756 m	3.5 h	1756 m	1.8 h
	2736 m	8.0 h	2524 m	5.1 h	2524 m	2.5 h
	4050 m	8.0 h	3292 m	6.6 h	3292 m	3.3 h
$\Gamma_c = 15$ dB	828 m	8.0 h	806 m	4.5 h	806 m	2.2 h
	1696 m	8.0 h	1440 m	8.0 h	1433 m	4.0 h
	2737 m	8.0 h	2231 m	8.0 h	2061 m	5.8 h
	4050 m	8.0 h	3120 m	8.0 h	2688 m	7.5 h
$\Gamma_c = 20$ dB	828 m	8.0 h	729 m	8.0 h	698 m	5.5 h
	1696 m	8.0 h	1440 m	8.0 h	1280 m	8.0 h
	2737 m	8.0 h	2231 m	8.0 h	1932 m	8.0 h
	4050 m	8.0 h	3120 m	8.0 h	2670 m	8.0 h

Table 2. Resolutions at $\lambda = 3$ mm (100 GHz) of the configurations for the three different specifications on the level of truncation of the clean weighting function as given by Eq.A.2 with $\beta = 1$ (no extrapolation).

	200 m	900 m	1600 m	2300 m	3000 m	10 km
$\Gamma_c = 10$ dB	2.49″	0.55″	0.31″	0.22″	0.17″	0.05″
$\Gamma_c = 15$ dB	3.05″	0.68″	0.38″	0.26″	0.20″	0.06″
$\Gamma_c = 20$ dB	3.52″	0.78″	0.44″	0.31″	0.23″	0.07″

Table 3. Resulting number of pads after the optimization of 5 configurations (1 compact and 4 intermediates) for various combinations of sampling constraint, α, and cut off of the clean weighting function, Γ_c.

	$\alpha = 1$	$\alpha = 2$	$\alpha = 4$
$\Gamma_c = 10$ dB	241	226	214
$\Gamma_c = 15$ dB	236	218	205
$\Gamma_c = 20$ dB	237	216	205

constraint for all the configurations but this is not necessary. It is, for example, possible to choose a stronger sampling constraint for the compact configurations than for the extended ones. It is also noticeable that the durations of the observations required for $\Gamma_c = 15$ dB are more realistic than for $\Gamma_c = 20$ dB whereas the number of pads required is comparable.

From all these considerations it was decided for the following to take $\Gamma_c = 15$ dB and $\alpha = 2$ for the first intermediate configuration, and $\Gamma_c = 15$ dB and $\alpha = 4$ for the 3 other intermediate configurations.

4. The intermediate configurations

This section shows the results of the optimization of 4 intermediate configurations with the ground constraints corresponding to the topography of Chajnantor. The digital mask described in Butler (2001) is used to exclude the pads from the regions where the slope is too steep (> 5 deg). The center of the compact configuration is situated at "Chajnantor South" as specified by the PDR (Guilloteau & the Configuration PDR Review Committee 2001). As justified in the previous section the parameters taken for the determination of the widths of the target distributions and of the durations of the observations are

$\alpha = 2$ (distance between the samples smaller than twice the Nyquist interval) for the first intermediate configuration, $\alpha = 4$ (distance between the samples smaller than four times the Nyquist interval) for the others and $\beta = 1$ (no extrapolation allowed in the imaging process) and $\Gamma_c = 15$ dB (level of truncation specified for the Fourier transform of the clean beam) for all of them.

The resulting configurations are shown in the figures E.6, E.7, E.8 and E.9. The total resulting number of pads for the intermediate and the compact configurations is of 196. The beams of the four intermediate configurations are shown in the Figures E.12, E.13, E.14 and E.15. In each figure two beams are shown: one obtained with the natural weighting and the other obtained with a weighting compensating for defects in the distribution of samples and such that the loss of sensitivity is of 5% (see Appendix B). Note that such a weighting allows to get a level of sidelobes lower than 2% almost everywhere. It is important to note that to compensate for the defects in the distribution the density was calculated at the scale of Nyquist interval. This leads to the fundamental result that most of the sidelobes are due to the defects in the distribution at the scale of Nyquist interval not to resonances in the coordinates of the samples (as is expected for distributions in which most of the samples are closer to each other than Nyquist interval). It is therefore justified to address the problem of the design by optimizing the configurations for distributions of samples without paying attention to possible resonances in the exact coordinates. This would of course be different for distributions in which most of the distances between the neighboring samples would be greater than Nyquist interval.

The defects in the distribution of samples can be due, either to the fact that the configuration is not really optimal (e.g. the number of iterations or the number of grids used in the optimization is not sufficient) or to an intrinsic limit to the quality of the distribution (e.g. due to the nature of the distribution of samples (see e.g. Woody 2001) or the topographic constraint). Although APO software cannot guarantee the solution obtained to be the absolute optimal one, the number of iterations was taken sufficiently large to believe that most of the defects are due to the second reason. The number and the size of the grids were also adjusted carefully .

Moreover, it should be emphasized that it is precisely when most of the uv-domain is sampled at a rate close to Nyquist rate that the sidelobes have the less impact in the image reconstruction process. In a simplified picture the problem is shifted from a fitting problem in the image or Fourier plane to a weighting problem in the Fourier plane. Then, the relevant parameter that allows to evaluate the quality of a configuration is not the level of sidelobes but rather the loss of sensitivity implied by a weighting that "cleans" the beam. Here we can see that for a 5% loss most of the unpleasant features disappear.

5. The extended configuration

In the case where no prior information on the source are available but mosaicing is allowed (i.e. $\alpha = 2$ in the terminology of Paper II) and where the maximum duration of observation is of 8 h, the largest possible baseline length is equal to 9.8 km (see Appendix A). It is therefore well justified to build an extended configuration of 10 km in diameter. The corresponding FWHM of the target Gaussian distribution is of 20 km (this corresponds to a truncation level of 3 dB). Because of the topological constraints the extended configuration should anyway be off-centered from the intermediate configurations and the sharing of the pads cannot be expected to be high. Therefore, the requirement that the configuration should be centrally concentrated does not hold for the extended configuration and designing a configuration for such a flat distribution is justified.

A configuration optimized for such a distribution is shown Fig.E.10. It forms a kind of ring around Cerro El Chascon. It uses 53 more pads, which leads to a total number of pads exactly equal to 249. Note that the same digital mask as for the intermediate configurations was used for the topological constraint. The synthesized beam is represented in Fig.E.16 and as in previous section it can be seen that most of the structure of the sidelobes disappear at the expense of 5% of the sensitivity. This configuration is an alternative to the recommendation of the PDR for a 14km-configuration.

6. Conclusion

An array of 249 pads was optimized following the recommendations of the PDR. The characteristics of the optimized configurations are summarized in Table 4. The optimization was performed using the APO software described in Paper I and conforming to the analysis of Paper II (whose results are summarized in Appendix A). The total computing time to get the complete array is of about 3 hours on a 1 GHz PC.

It was demonstrated that a compact configuration could be optimized taking into account the problems of the access to the antennas and of the shadowing. Then, it was shown that, if four intermediate configurations are wanted, the constraint on the total number of pads requires some of the intermediate configurations to be optimized for a sampling rate four times lower than Nyquist rate at the edges of the distribution of samples and for a truncation level of 15 dB. Locations of the pads were found for four intermediate configurations on the 5 degree mask. Finally it was shown that an extended configuration of 10 km in diameter would fit on the 5 degree mask around Cerro El Chascon. The quality of all the configurations was checked: for a 5% loss of sensitivity it is possible to remove most of the sidelobes by weighting properly the data.

These results demonstrate that it is possible to base the design of ALMA on an inverse approach. In such an

Table 4. Characteristics of the configurations. The resolutions given are the FWHM of the Fourier transform of the Gaussian distributions whose FWHM are given in the second column except for the extended configuration: it is computed for a weighting such that $\Gamma_c = 15$ dB.

config.	largest baseline	FWHM of target dist.	duration of the obs.	sampling α	truncation level	resolution @100 GHz
compact	200 m	200 m	1.2 h	1	12 dB	3.05″
1rst	900 m	806 m	4.5 h	2	15 dB	0.68″
2nd	1600 m	1433 m	4.0 h	4	15 dB	0.38″
3rd	2300 m	2061 m	5.8 h	4	15 dB	0.26″
4th	3000 m	2670 m	7.5 h	4	15 dB	0.20″
extended	10 km	20 km	8 h	2	3 dB	0.06″

approach the locations of the pads are determined by the scientific goals translated in terms of target distributions of samples. The method used allows at the same time to control the quality of the distribution of samples (shape and minimum density of samples) and to take into account the constraints and specifications (topography, number of pads, range of resolutions).

It is emphasized that the positions of the pads were obtained without any human intervention. The process is automated, it can be repeated indefinitely and the various parameters adjusted as wanted. This aspect is important as new constraints may appear or the specifications may evolve during the conception and the construction of the instrument. With the software used here new positions can be easily and rapidly obtained, the design does not correspond to a fixed concept but rather to an adaptable response to some requirements and specifications. The main parameters that can be changed are:

- for the compact configuration: the constraint on the shadowing, the design of the road tracks.
- for the other configurations: the number of configurations (for example 3 intermediate configurations instead of 4), the sampling constraint and the truncation level for each configuration. The maximum duration of observations (in Holdaway (1998) 4 hours is recommended rather than 8 hours, this would have an impact on the 4th intermediate configuration and on the extended one).

Some improvement might also be brought by changing the initial conditions of the optimization. For each intermediate configuration the initial configuration used as input in the software was the previous configuration in the increasing size order. It can be seen for example that the first intermediate configuration undergoes strong topographic constraints on the North-West (see Fig.E.6). It could probably be improved if the initial configuration was shifted by 100 meters toward the East. It should also be noted that for the extended configuration the complicated topographic constraints might be able to "trap" some of the antennas. It is therefore possible that the quality of the final configuration depend upon the initial conditions, i.e. the input configuration. It could therefore be possible to improve the result by optimizing a great number of different initial configurations and select the best result.

Some aspects that should be considered to validate definitely a design were not considered here: the reconfiguration scenario, the positions of additional antennas (in theory there could be as much as 64 antennas), the effect of missing antennas, the design of the roads and the wiring. Note that the former two issues can be addressed using the APO software. Indeed the reconfiguration scenario can be derived by:

- allowing one antenna only to move (e.g. the one undergoing the strongest pressure),
- optimizing the configuration for a maximum baseline length incremented by a small amount,
- putting the antenna on the nearest pad,
- iterating.

The locations of additional antennas could be determined in the same way.

References

Boone, F. 2001, A&A, 377, 368
—. 2002, submitted
Briggs, D. S. 1995, PhD thesis, The New Mexico Institute of Mining and Technology
Butler, B. 2001, in ALMA memo No. 364
Conway, J. 2000, in ALMA memo No. 292
Guilloteau, S. & the Configuration PDR Review Committee. 2001
Holdaway, M. A. 1998, in ALMA memo No. 201
Woody, D. 2001, in ALMA memo No. 389

Appendix A: Derivation of the target distributions

This appendix summarizes the results of Paper II.

The distribution of samples in the Fourier plane that should be taken as target when optimizing an array for imaging is determined by:

- the "work" that can be demanded to the image reconstruction process (i.e. the levels of interpolation and extrapolation that can be achieved),

– the level of sidelobes tolerated in the clean map,
– the resolution wanted in the clean map.

The work that can be demanded to the imaging process can be characterized by 2 parameters α and β representing respectively the level of interpolation and extrapolation that can be demanded to the imaging process:

$$\alpha = \frac{\delta u_M}{\delta u_o}, \text{ and } \beta = \frac{\Delta u_e}{\Delta u_s}, \quad \text{(A.1)}$$

where

– δu_M is the sampling accuracy (exact definition in paper II) required to allow estimation of the visibility function within the sampled uv-region.
– δu_o is the Nyquist interval: $\delta u_o = 1/\Delta\theta_{PB}$, where $\Delta\theta_{PB}$ is the angular size of the primary beam.
– Δu_s is the radius of the sampled uv-disc.
– Δu_e is the radius up to which the visibility function can be reasonably extrapolated.

When no prior information on the source are available and single field observations are made Nyquist sampling is required i.e. $\alpha = 1$. When mosaicing is allowed it is possible to recover the value of the visibility function around the samples of a single field up to a radius equal to δu_o. One can therefore interpolate between samples that are separated by $2\delta u_o$ i.e. $\alpha = 2$.

The *clean weighting function* is defined as the Fourier transform of the wanted clean beam. The level of sidelobes in the clean map is directly related to the truncation level of the clean weighting function. Let γ_c be this truncation level and Γ_c its value in dB. At a given wavelength specifying a resolution is equivalent to specifying a size for the array. For Gaussian distributions of samples truncated at a low level the largest projected baseline of the array B is related to the resolution in the clean map $\delta\theta_c$ by:

$$\delta\theta_c = \frac{2\sqrt{b\ln 2}}{\pi} \frac{{\Gamma_c}^{\frac{1}{2}}}{\beta} \frac{\lambda}{B} \quad \text{with } b = \frac{\ln 10}{10}. \quad \text{(A.2)}$$

Then, for an array of n_a antennas of diameter D and for a maximum duration of observation in hour Δt_{max}, two characteristic baseline lengths are introduced:

$$B_o = \frac{n_a(n_a-1)\,\alpha\, D\, \Delta t_{max}}{48\,\chi} \quad \text{(A.3)}$$

where $\chi = \frac{\beta^2}{b\Gamma_c}\left[\exp\left(\frac{b\Gamma_c}{\beta^2}\right) - 1\right]$ and,

$$B_{max} = \frac{n_a(n_a-1)\,\alpha\, D\, \Delta t_{max}}{48 \times 1.44}. \quad \text{(A.4)}$$

The first baseline length corresponds to the largest array size allowing single configuration observations without loss of sensitivity and the second one to the largest array size allowing single configuration observations. For larger sizes image reconstruction is in principle not possible and multicofiguration observations are required.

For example if we take $\alpha = \beta = 1$ (i.e. no particular deconvolution algorithm and no prior information available), $\Gamma_c = 10$ dB and $\Delta t_{max} = 8$ h then we get : $B_o = 1.8$ km and $B_{max} = 4.9$ km for 60 antennas of 12 m. For $\alpha = 2$ we get $B_{max} = 9.8$ km. The latter value justifies an extended configuration of 10 km in diameter for ALMA.

Then, depending on the size of the array, three cases have to be considered:

1. $B < B_o$: the array can be optimized for a distribution of samples equal to the Fourier transform of the wanted clean beam. If the wanted clean beam is Gaussian then the FWHM, δ_c, of the target distribution is given by:

$$\delta_c = \frac{\beta}{a\sqrt{2b\Gamma_c}} \frac{B}{\lambda} \quad \text{where } a = \frac{1}{2\sqrt{2\ln 2}} \quad \text{(A.5)}$$

The duration of the observation required is then given by:

$$\Delta t = \frac{48\,\chi\, B}{n_a(n_a-1)\,\alpha\, D}. \quad \text{(A.6)}$$

2. $B_o < B < B_{max}$: the duration of observation is maximum. To allow the uv-disc to be well sampled everywhere and to minimize the loss of sensitivity the array should be optimized for a wider Gaussian distribution of samples (for a higher truncation level). The FWHM, δ_s, of the target distribution of samples is solution of:

$$\frac{2a^2\lambda^2\delta_s^2}{B^2}\left[\exp\left(\frac{B^2}{2a^2\lambda^2\delta_s^2}\right) - 1\right] - \frac{B}{1.44\,B_{max}} = 0 \quad \text{(A.7)}$$

3. $B > B_{max}$: the array should be optimized for multiconfiguration observations.

Appendix B: Weighting

Two kinds of weighting are used in this memo: the natural weighting and a weighting that compensates for the defects in the distribution of samples. For natural weighting the weights are proportional to the inverse variance of the data:

$$w_{Ni} = \frac{C}{\sigma_i^2} \quad \text{(B.1)}$$

where C is a constant. In this memo the variance of the data is taken proportional to the system temperature which is assumed to depend on the airmass only.

The idea that the sidelobes are partly due to defects in the distribution of samples is well known (see e.g. Woody 2001) and weighting the data in a way that compensates for these irregularities is not new (see e.g. Briggs 1995). The simplest way to compensate for the density excess with respect to an ideal distribution is to weight each data by:

$$w_{oi} = \frac{d_m(u_i,v_i)/d(u_i,v_i)}{\max\left(d_m(u_i,v_i)/d(u_i,v_i), i\right)}, \quad \text{(B.2)}$$

where $d(u_i,v_i)$ is the local density of weights (i.e. density of samples affected by their natural weights) at the coordinates (u_i,v_i) of the i^{th} sample and $d_m(u_i,v_i)$ the density it should be in an ideal Gaussian distribution of a given

truncation level. Note that these weights are normalized such that the maximum is equal to 1. The loss of sensitivity induced by such a weighting might however be too important and it is possible to control the values of w_i in order to find a good compromise. One way to do that is to fix a floor for the weights and define them as follows:

$$w_{Fi} = \begin{cases} w_{oi} & \text{if } w_{oi} \geq F \\ F & \text{if } w_{oi} < F \end{cases} \quad \text{(B.3)}$$

where F is a floor to be adjusted between 0 and 1. The higher the floor the lower the loss of sensitivity. Another way to control the loss of sensitivity is to use a coupling factor such that the weights are given by:

$$w_{Gi} = G(w_{Fi} - 1) + 1 \quad \text{(B.4)}$$

where G is to be adjusted between 0 and 1 to control the coupling of the weights to the density excess (1 is full coupling). The lower the value of G the less the sensitivity lost. In Sect.4 the beams are shown for natural weighting and for a weighting as given in the latter equation with F and G adjusted such that the loss of sensitivity equals 5%.

Appendix C: Loss of sensitivity

The transfer function S is defined as the sum of Dirac's delta-functions centered at the samples coordinates (u_i, v_i) and affected by some arbitrary weights, w_i:

$$S = \sum_i^N w_i \, \delta(u - u_i, v - v_i) \quad \text{(C.1)}$$

The choice of the weights allows to control the shape of the synthesized beam and thus to reduce the level of sidelobes. But the weights also affect the sensitivity of the reconstructed image. The minimum noise is obtained for a natural weighting. When the weighting applied is different from the natural weighting the relative loss of sensitivity on a centered point source is given by (Briggs 1995):

$$W = \frac{\sqrt{\sum w_{Ni}}}{\sum w_{Ni}} \sqrt{\sum \frac{w_i^2}{w_{Ni}}} - 1 \quad \text{(C.2)}$$

Appendix D: Mean declination, mean elevation and shadowing constraint

To derive the mean elevation we consider a uniform distribution of sources over the celestial sphere. Then the density of sources as a function of declination and such that it is normalized to 1 is given by:

$$w(\delta) = \frac{\cos\delta}{2} \quad \text{(D.1)}$$

If the lowest declination observable is δ_l and the highest δ_h, then the mean declination is given by:

$$\delta_m = \frac{\int_{\delta_l}^{\delta_h} \delta w(\delta) d\delta}{\int_{\delta_l}^{\delta_h} w(\delta) d\delta} \quad \text{(D.2)}$$

For Chajnantor site situated at a latitude $l = -23\,\text{deg}$ if observations at elevations lower than 20 deg are not permitted then $\delta_l = -90\,\text{deg}$ and $\delta_h = 47\,\text{deg}$. The corresponding mean declination is:

$$\delta_m \simeq -10\,\text{deg} \; . \quad \text{(D.3)}$$

The elevation is defined as $\epsilon = \frac{\pi}{2} - |\delta - l|$ where l is the site latitude.

$$\epsilon_m = \frac{\int_{\delta_l}^{\delta_h} \epsilon \, w(\delta) d\delta}{\int_{\delta_l}^{\delta_h} w(\delta) d\delta} \quad \text{(D.4)}$$

For Chajnantor site we get:

$$\epsilon_m \simeq 60\,\text{deg} \, . \quad \text{(D.5)}$$

To avoid shadowing, two antennas of diameter D, aligned to the north-south direction have to be separated by a distance d given by:

$$d(\epsilon) = \frac{D}{\sin\epsilon} \quad \text{(D.6)}$$

The mean value of this distance for the given distribution of sources is given by:

$$d_m = \frac{D}{\cos l} \frac{\int_{\delta_l}^{\delta_h} (1 + \tan l \tan\delta)^{-1} \, d\delta}{\sin\delta_h - \sin\delta_l} \quad \text{(D.7)}$$

with

$$\int (1 + a\tan\delta)^{-1} \, d\delta = \frac{\delta + a\ln(\cos\delta + a\sin\delta)}{1 + a^2} \quad \text{(D.8)}$$

For Chajnantor we obtain: $d_m = 1.3D$. The elevation, ϵ_{sh} such that $d(\epsilon_{sh}) = d_m$ is:

$$\epsilon_{sh} \simeq 50\,\text{deg} \; . \quad \text{(D.9)}$$

Appendix E: Figures

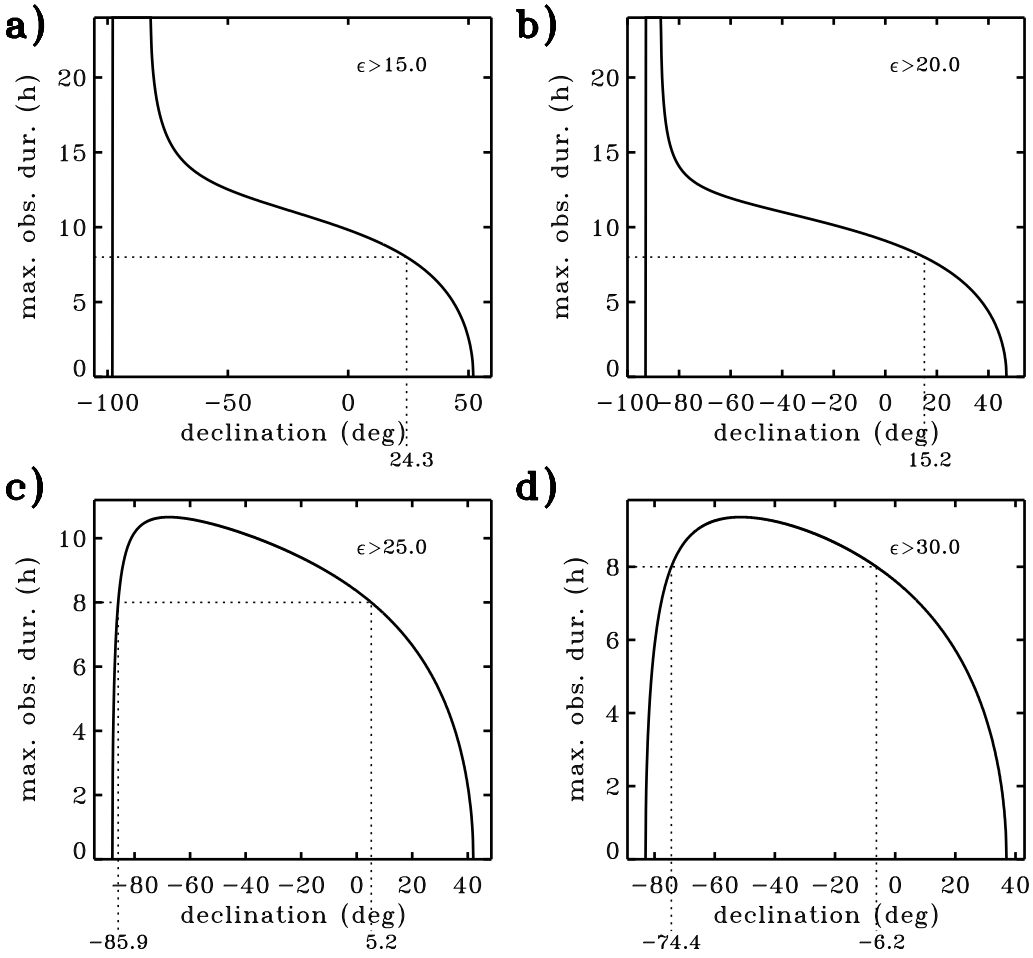

Fig. E.1. This figure shows the maximum possible hour angle range vs the declination of the source for a site latitude of −23 deg and for various limits on the minimum elevation, ϵ: **a)** $\epsilon > 15$ deg, **b)** $\epsilon > 20$ deg, **c)** $\epsilon > 25$ deg and **d)** $\epsilon > 30$ deg. Note that the sources of declination in the range [−74.4 deg, 6.2 deg] are observable during eight hours at elevations greater than 30 deg, this represents 54% of the observable sources. It was therefore decided to optimize the configurations for a maximum duration of observation equal to 8 hours.

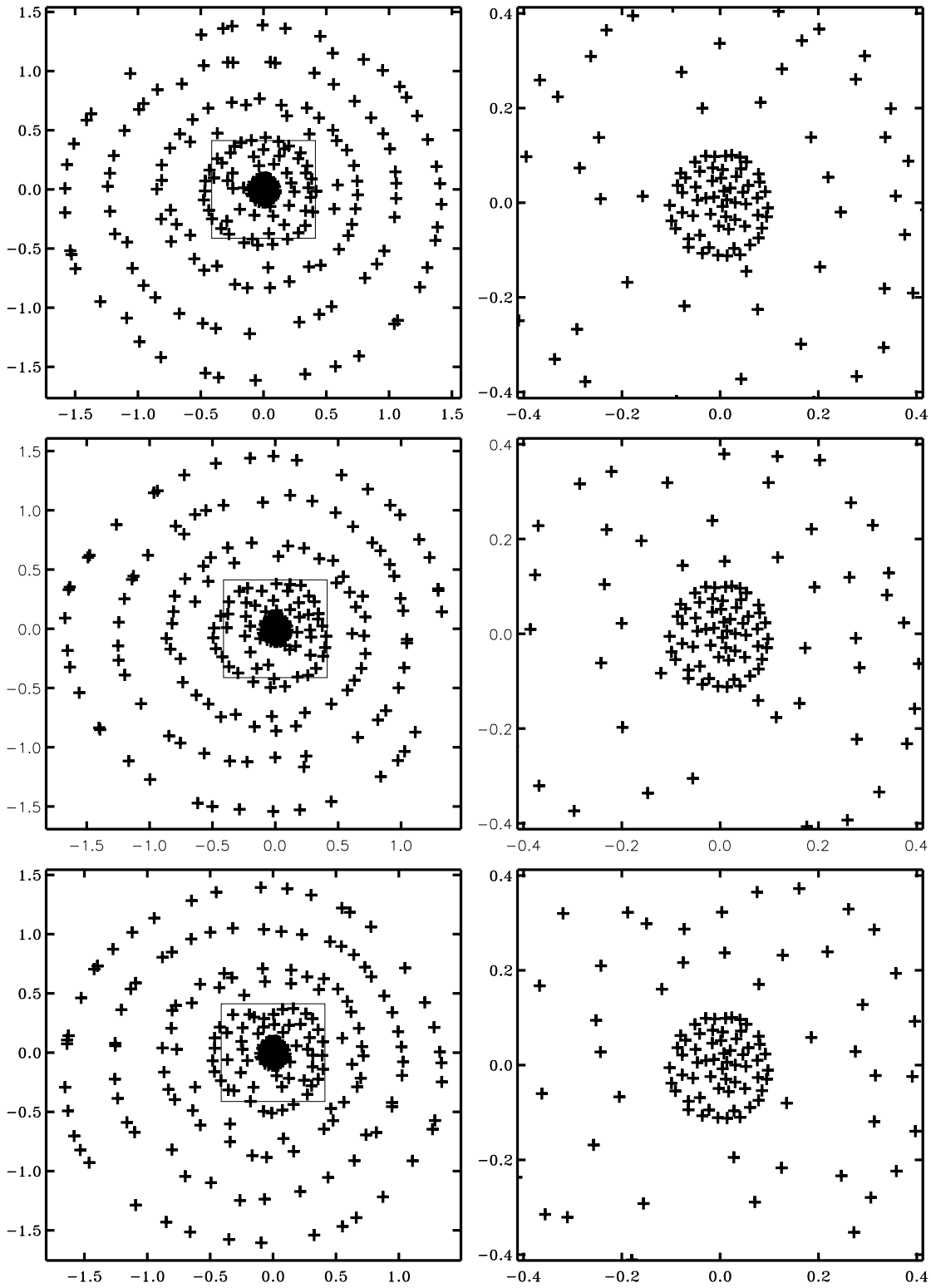

Fig. E.2. Arrays resulting from the optimization of 5 intermediate configurations (the compact one is described in Sect.2) for $\alpha = 1$ and Γ_c =10 dB (first row), 15 dB (second row) and 20 dB (third row). In each row the figure on the right-hand side is a zoom toward the center of the array.

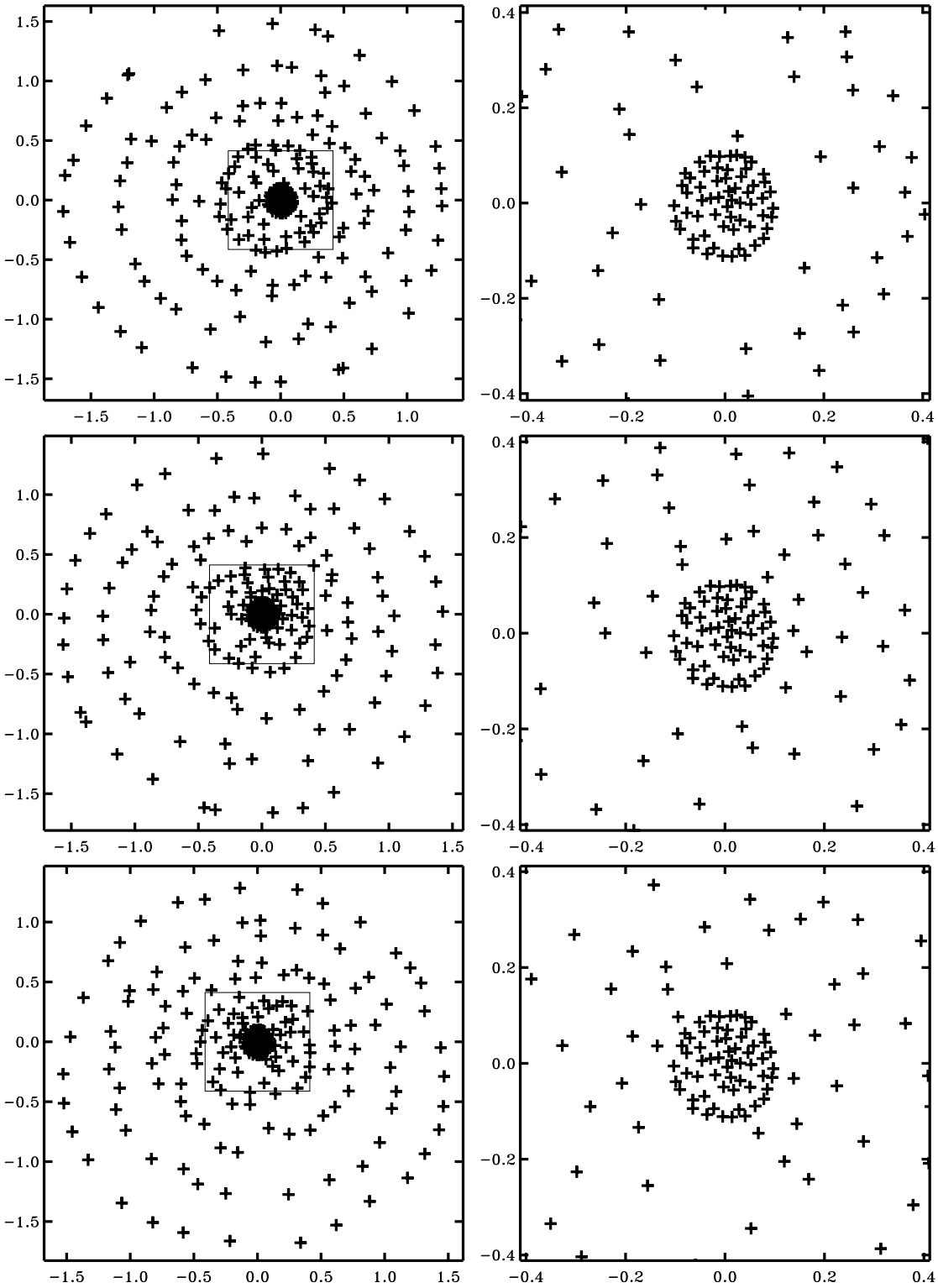

Fig. E.3. Arrays resulting from the optimization of 5 intermediate configurations (the compact one is described in Sect.2) for $\alpha = 2$ and Γ_c =10 dB (first row), 15 dB (second row) and 20 dB (third row). In each row the figure on the right-hand side is a zoom toward the center of the array.

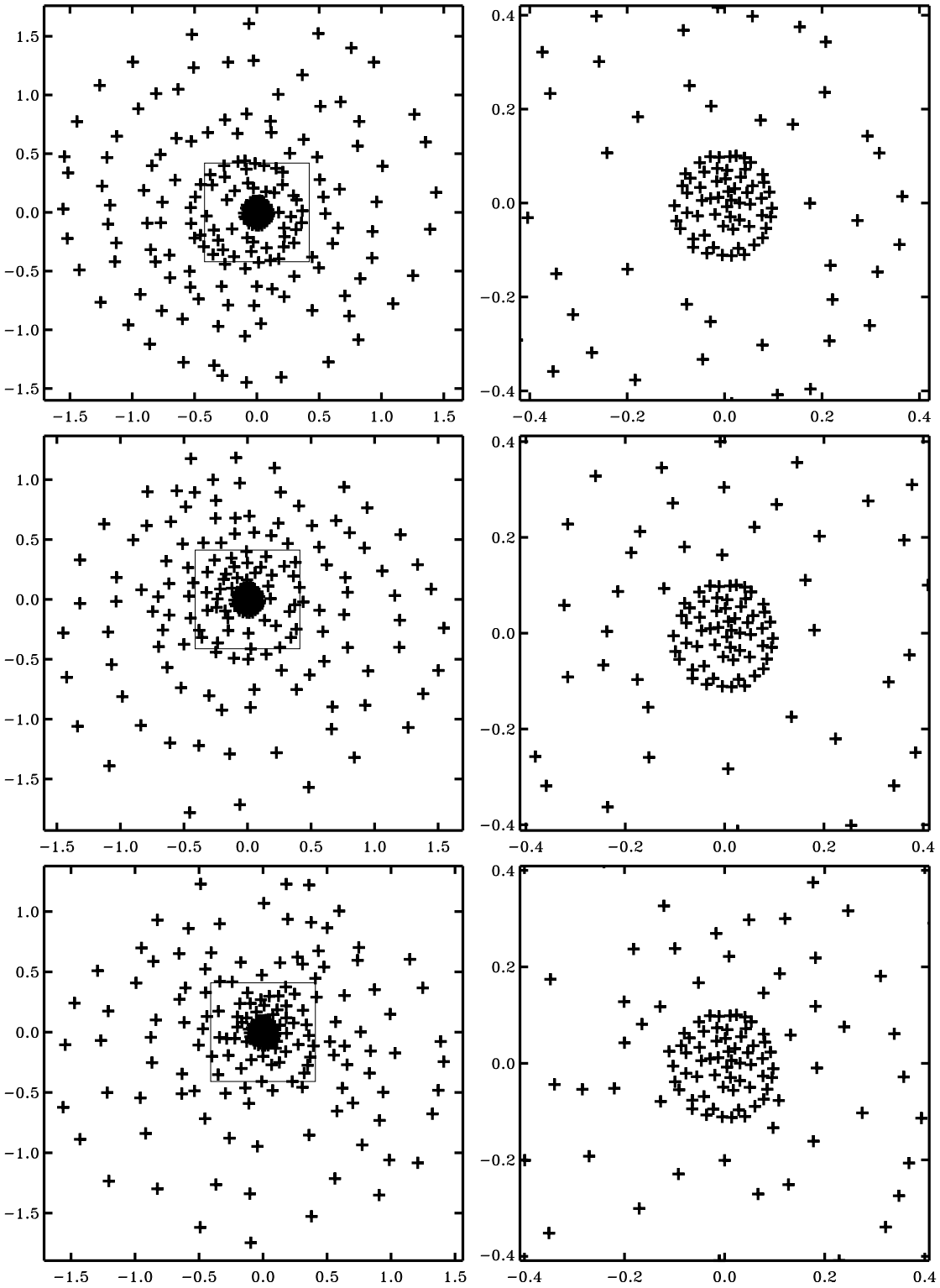

Fig. E.4. Arrays resulting from the optimization of 5 intermediate configurations (the compact one is described in Sect.2) for $\alpha = 4$ and Γ_c =10 dB (first row), 15 dB (second row) and 20 dB (third row). In each row the figure on the right-hand side is a zoom toward the center of the array.

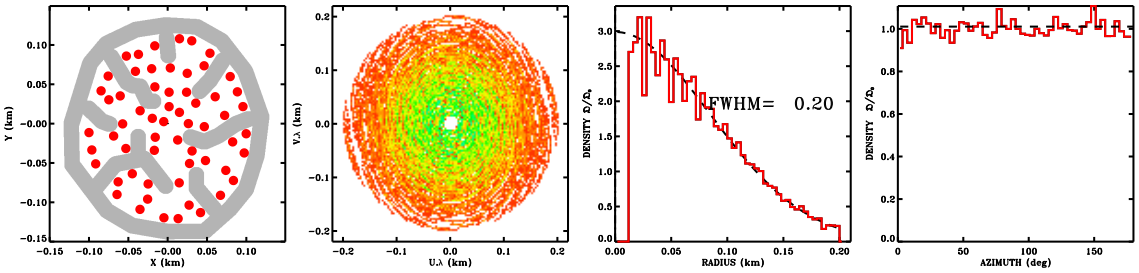

Fig. E.5. Compact configuration optimized for a Gaussian distribution of visibilities of FWHM= 200 m/λ (i.e. a truncation level of 12 dB) and for the mean source elevation ϵ_m = 60 deg. The inner boundary condition prevents any shadowing for elevations down to 50 deg.

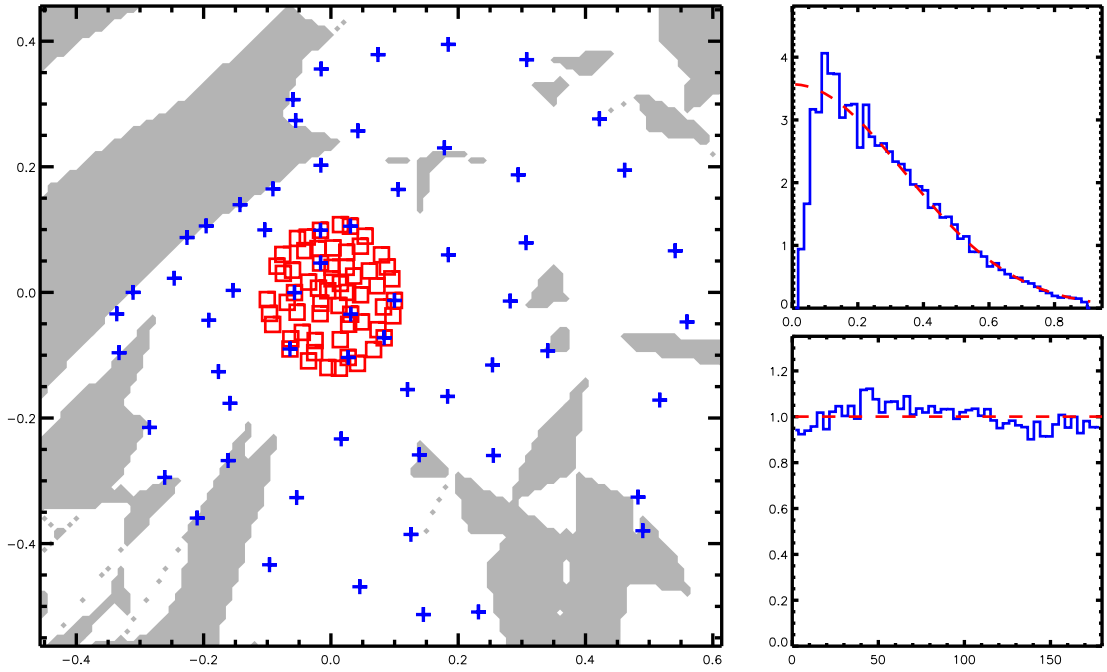

Fig. E.6. The blue crosses show the locations of the antennas in the first intermediate configuration. The red squares show the locations of the pads of the compact configuration. The figures on the right-hand side show the radial (top) and azimuthal (bottom) distribution of samples.

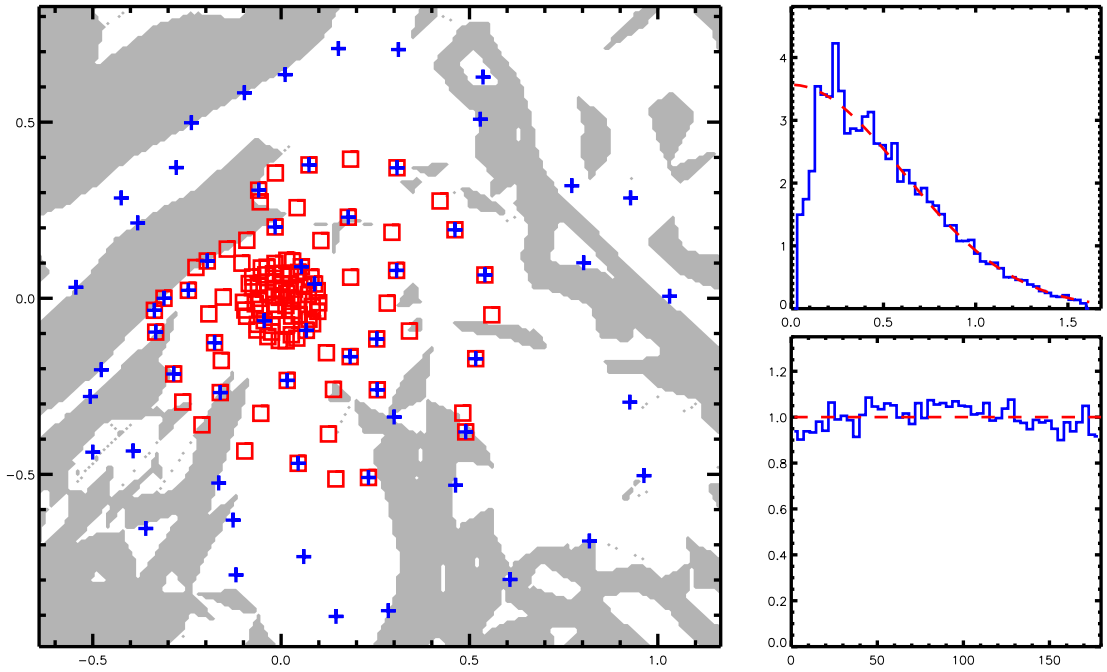

Fig. E.7. The blue crosses show the locations of the antennas in the second intermediate configuration. The red squares show the locations of the pads of the compact and first intermediate configurations. The figures on the right-hand side show the radial (top) and azimuthal (bottom) distribution of samples.

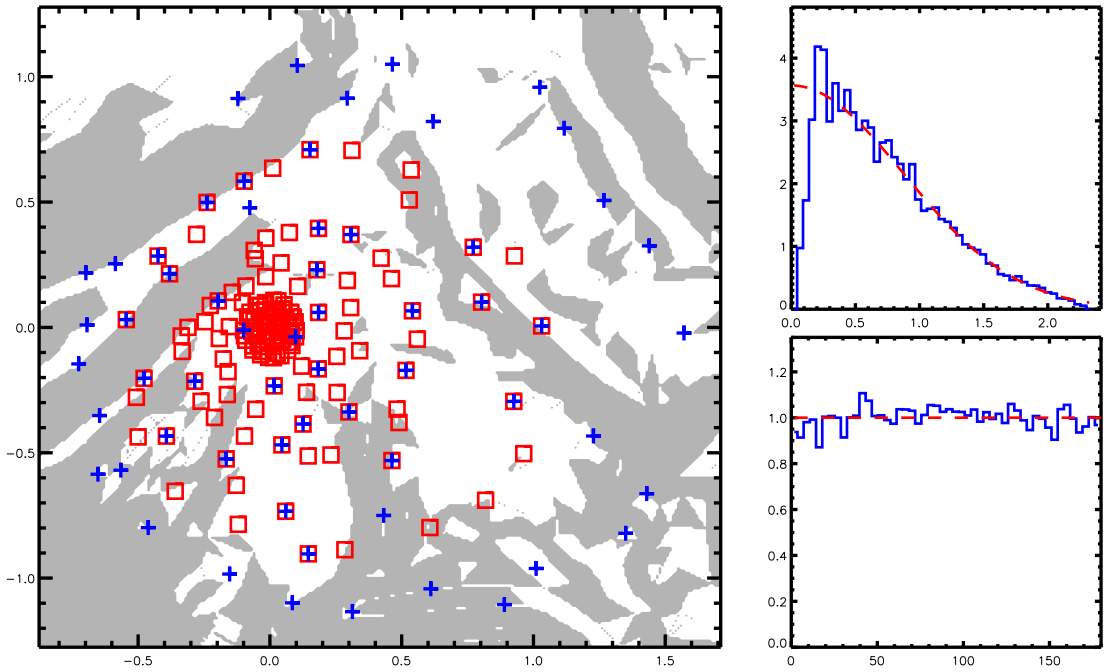

Fig. E.8. The blue crosses show the locations of the antennas in the third intermediate configuration. The red squares show the locations of the pads of the compact, the first and the second intermediate configurations. The figures on the right-hand side show the radial (top) and azimuthal (bottom) distribution of samples.

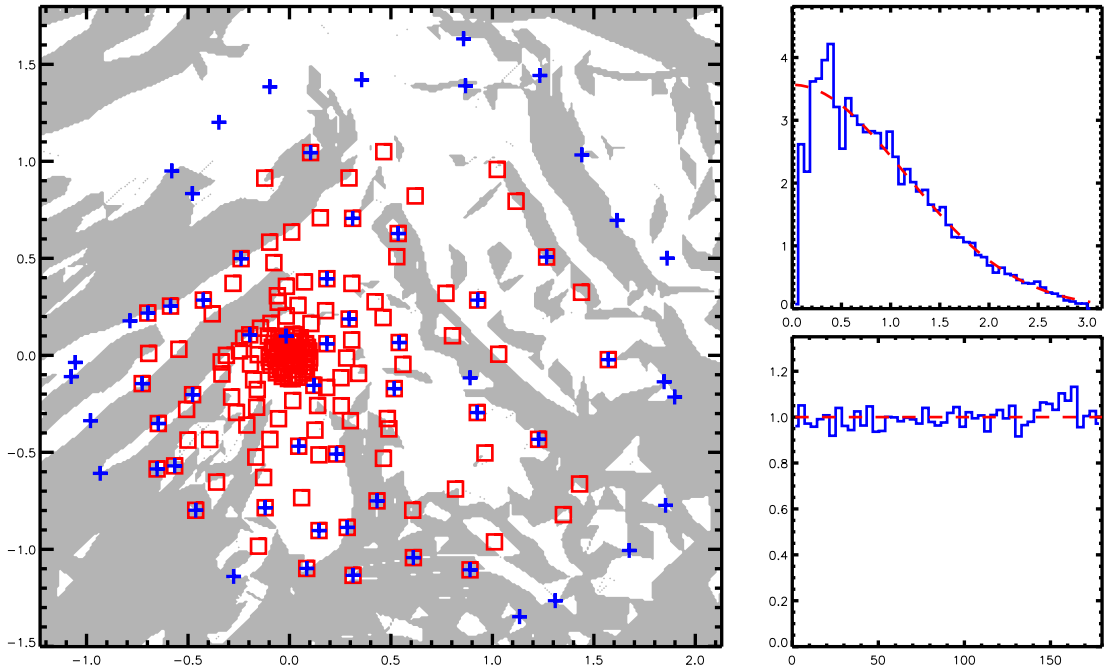

Fig. E.9. The blue crosses show the locations of the antennas in the fourth intermediate configuration. The red squares show the locations of the pads of the compact and the other intermediate configurations.

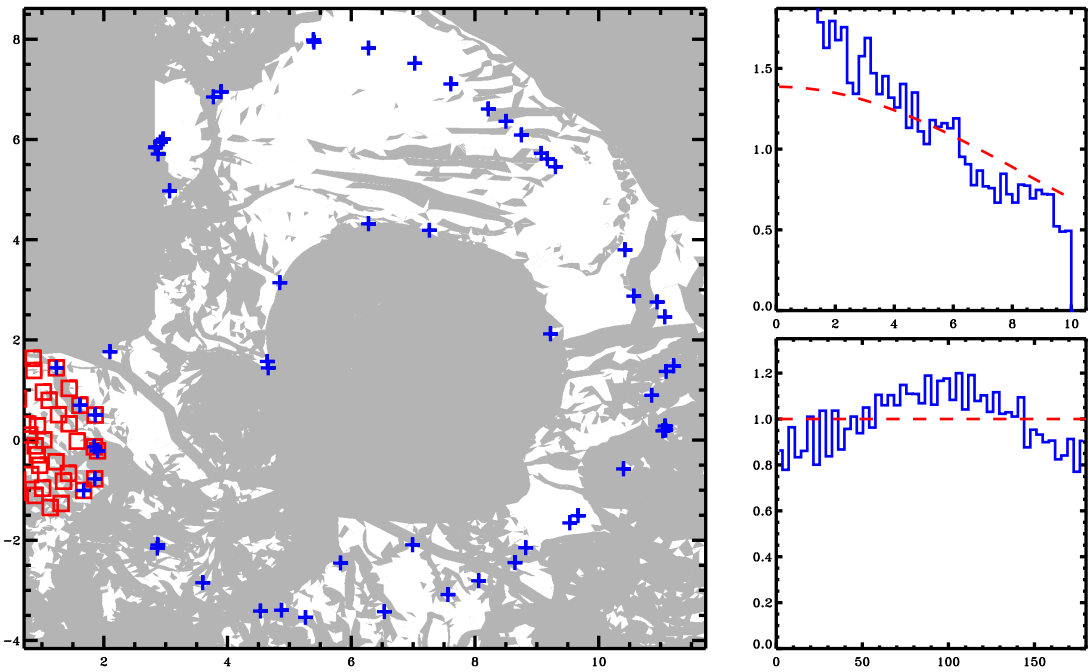

Fig. E.10. The blue crosses show the locations of the antennas in the extended configuration. The red squares show the locations of the pads of the compact and intermediate configurations. The figures on the right-hand side show the radial (top) and azimuthal (bottom) distribution of samples.

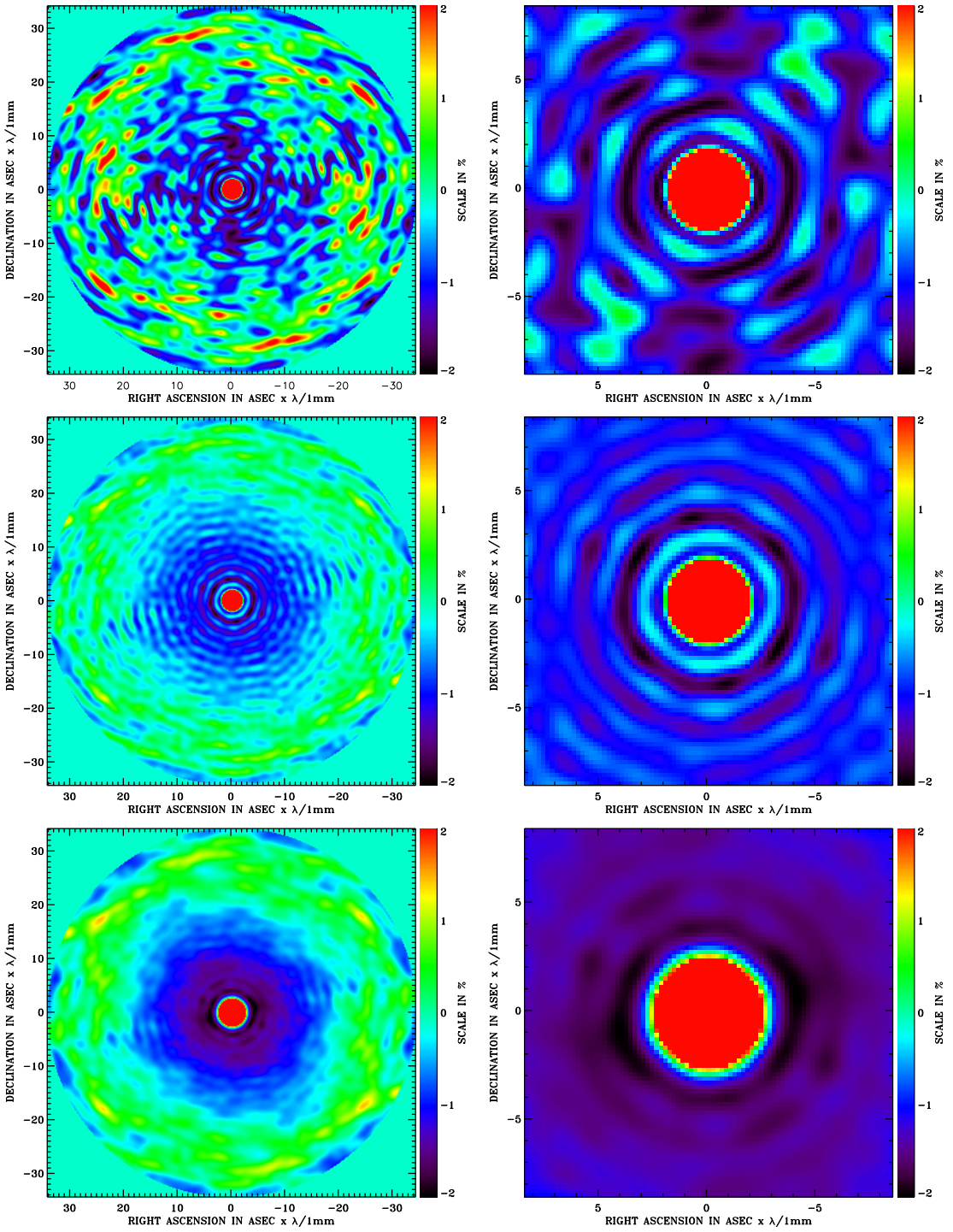

Fig. E.11. Dirty beams obtained with the compact configuration and with three different weightings. In each row the figure on the right-hand side is a zoom toward the central part of the beam. In the first row the weighting used is the so-called natural weighting. The second and last rows represent the beam after a weighting compensating for the excess of density with respect to a perfect Gaussian distribution of samples truncated at respectively 12 dB and 20 dB (see Appendix B). For these two cases the loss of sensitivity is respectively 5% and 10% (see Appendix C for computation).

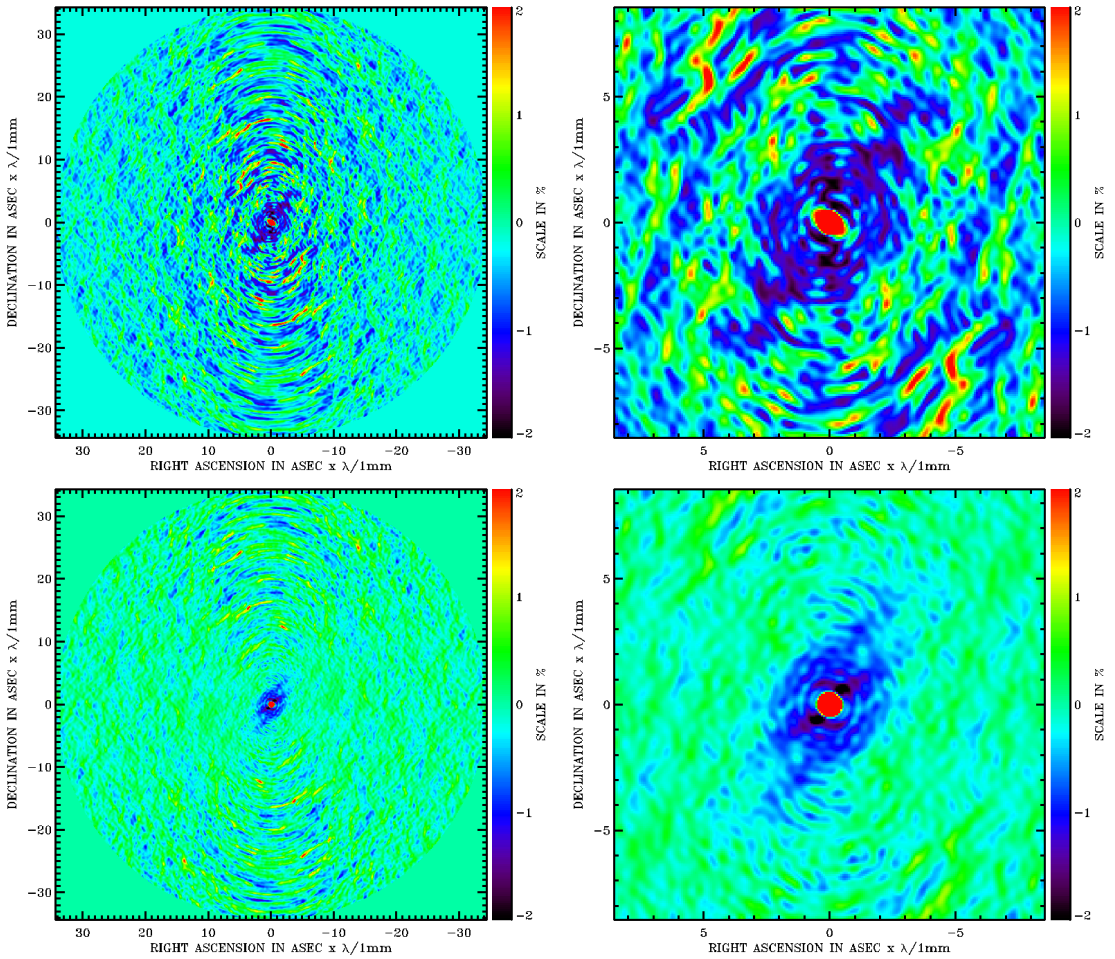

Fig. E.12. Dirty beam of the first intermediate configuration using the natural weighting (first row) and a weighting compensating for the excess of density with respect to a perfect Gaussian distribution truncated at 15 dB (second row). As described in Appendix B in the latter case the weights were adjusted such that the loss of sensitivity does not exceed 5%.

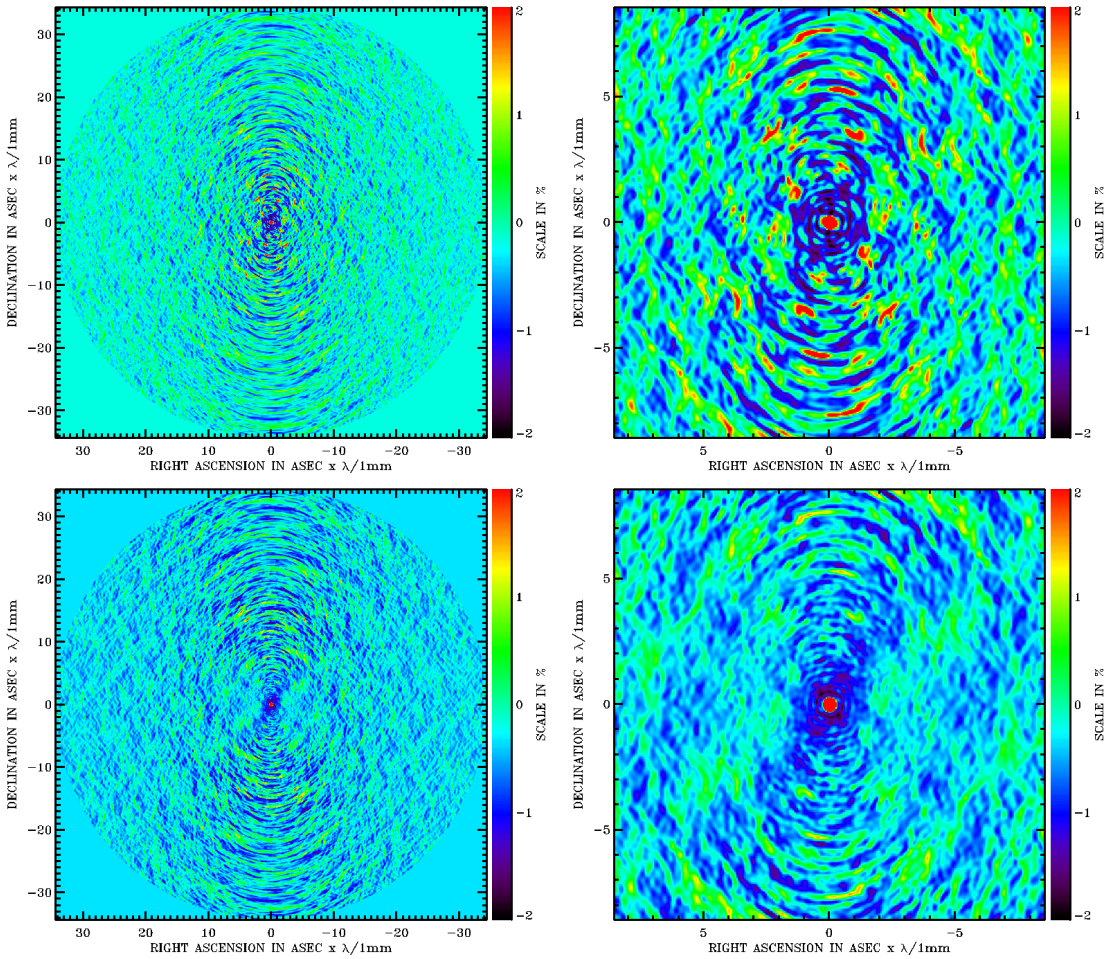

Fig. E.13. Dirty beam of the second intermediate configuration using the natural weighting (first row) and a weighting compensating for the excess of density with respect to a perfect Gaussian distribution truncated at 15 dB (second row). As described in Appendix B in the latter case the weights were adjusted such that the loss of sensitivity does not exceed 5%.

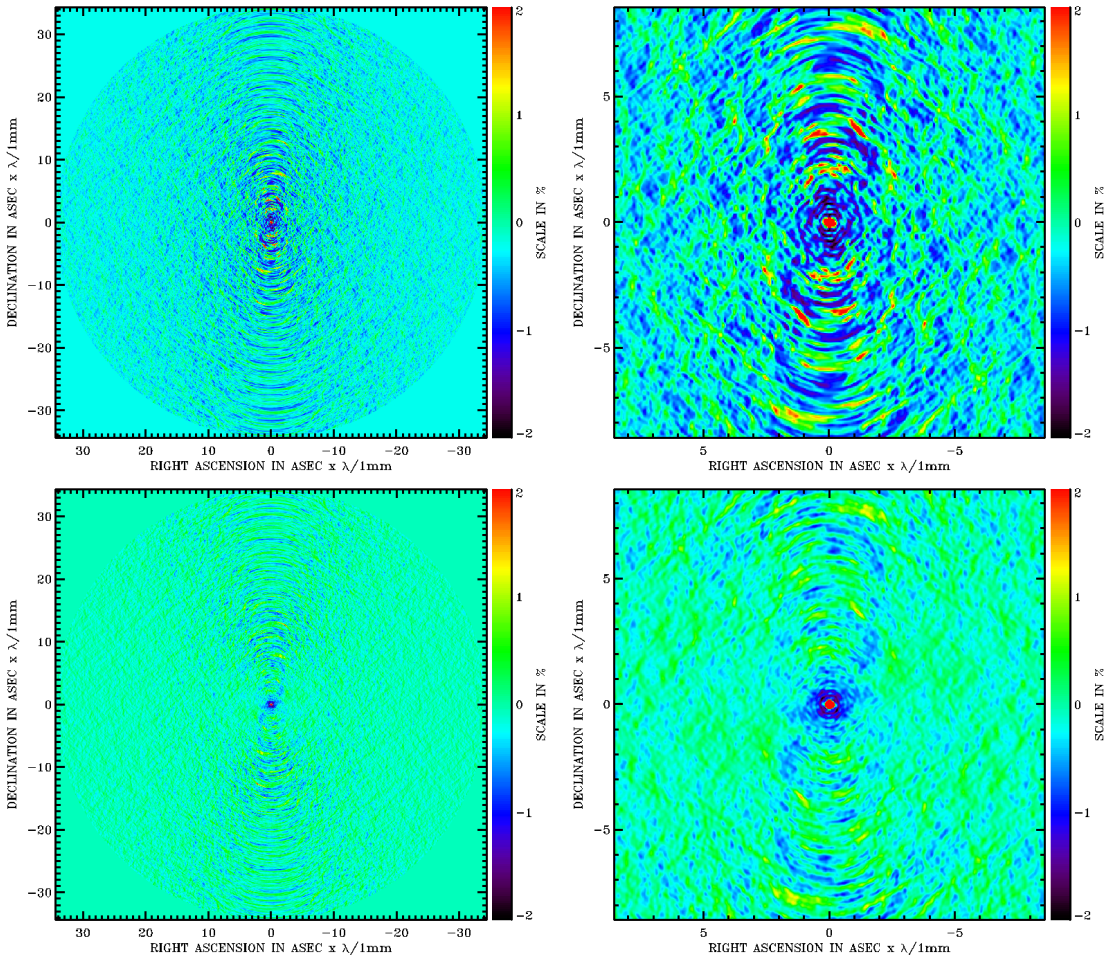

Fig. E.14. Dirty beam of the third intermediate configuration using the natural weighting (first row) and a weighting compensating for the excess of density with respect to a perfect Gaussian distribution truncated at 15dB (second row). As described in Appendix B in the latter case the weights were adjusted such that the loss of sensitivity does not exceed 5%.

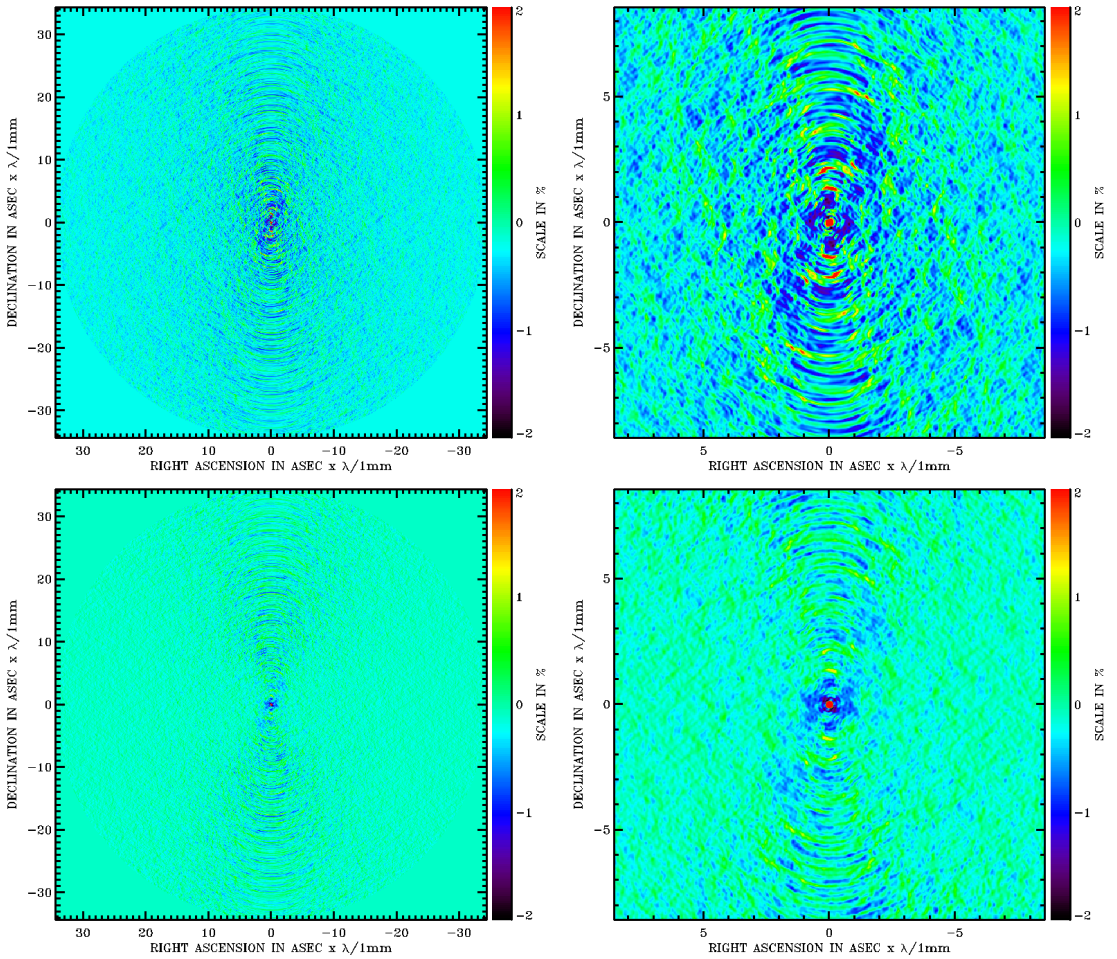

Fig. E.15. Dirty beam of the fourth intermediate configuration using the natural weighting (first row) and a weighting compensating for the excess of density with respect to a perfect Gaussian distribution truncated at 15 dB (second row). As described in Appendix B in the latter case the weights were adjusted such that the loss of sensitivity does not exceed 5%.

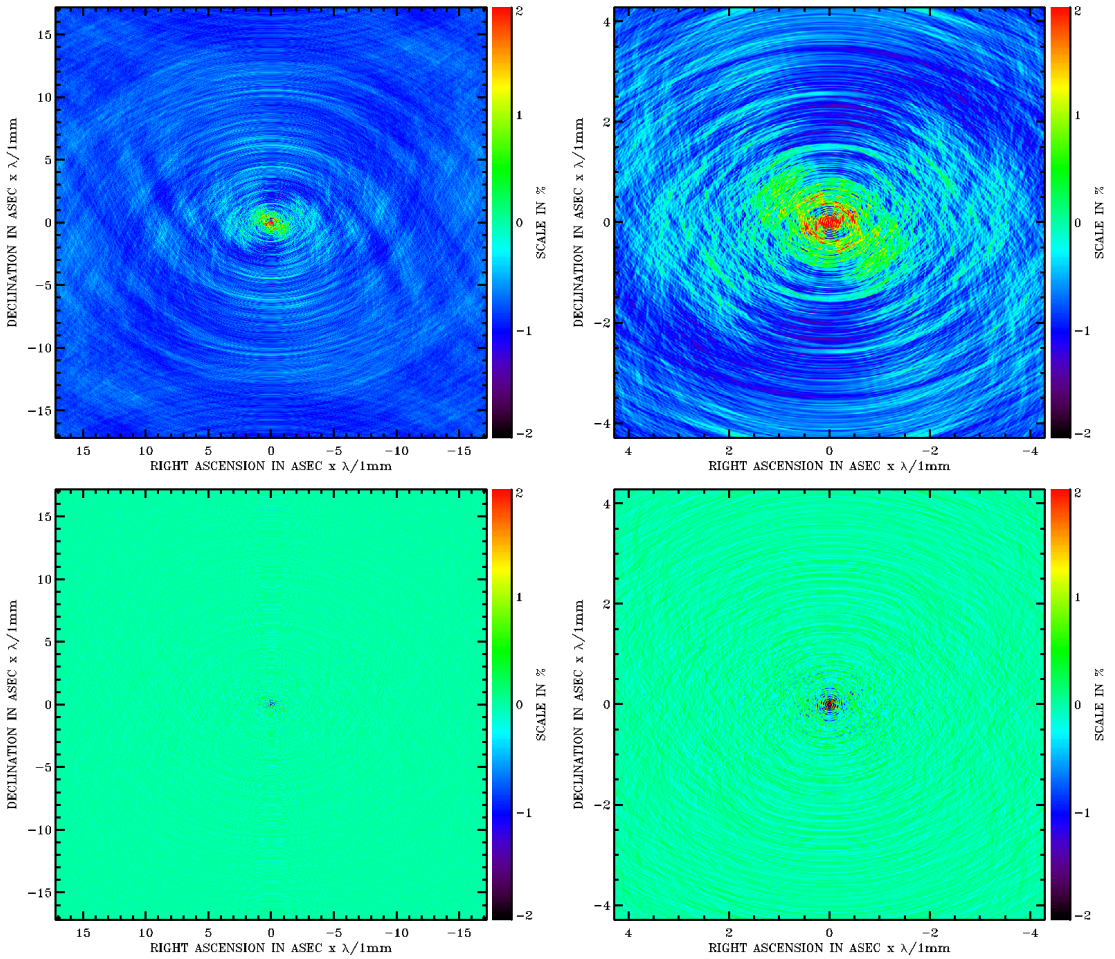

Fig. E.16. Dirty beam of the extended configuration using the natural weighting (first row) and a weighting compensating for the excess of density with respect to a perfect Gaussian distribution truncated at 3 dB (second row). As described in Appendix B in the latter case the weights were adjusted such that the loss of sensitivity does not exceed 5%.